J Mol Model (2010) 16:1–8
DOI 10.1007/s00894-009-0514-1

ORIGINAL PAPER

Explaining the inhibition of cyclin-dependent kinase 5 by peptides derived from p25 with molecular dynamics simulations and MM-PBSA

Vincent B. C. Tan · Bing Zhang · Kian Meng Lim · Tong Earn Tay

Received: 27 November 2008 / Accepted: 27 March 2009 / Published online: 23 May 2009

Abstract A cyclin-dependent kinase (CDK) 5 inhibitory peptide (CIP) from p25 was recently reported to inhibit CDK5/p25 activity in vitro but had no effect on endogenous cdc2 kinase activity. This may lead to a specific CDK5 inhibition strategy in the treatment of neurodegeneration. However, the mechanism of the inhibition remains unclear. In this work, molecular dynamics simulations and energy decomposition calculation models were set up to investigate the deregulation mechanisms of CIP on CDK5 activity. The results show that truncation of the N, and C terminals of p25 introduces important conformational changes into a hydrophobic pocket that is crucial for accommodating Ile153 on the activation loop of CDK5. In addition, such truncations lead to distortion and displacement of the activation loop and consequently affect binding of the substrate peptide. New inhibition sites for selectively inhibiting the activity of CDK5 are also suggested.

Keywords Molecular dynamics simulations · Cyclin-dependent kinase · Inhibition · Energy decomposition

Introduction

Cyclin-dependent kinases (CDKs) constitute a family of serine/threonine kinases. Their activity is regulated by interaction with activator proteins [1–6]. These protein kinases catalyze the phosphoryl transfer of the γ-phosphate group of ATP to serine, threonine, or tyrosine residues of protein substrates to trigger a series of downstream consequences [7–13]. According to reported crystallographic [14, 15] and theoretical structures, these CDKs have very similar three-dimensional (3D) structures as reflected in their very high sequence similarity. They all possess a fold comprising an N-terminal domain composed largely of a β-sheet with one helix, and a larger C-terminal domain composed of mostly α-helices. Although most CDKs in this family have been implicated in the regulation of the cell division cycle and are activated by cyclins, emerging evidence suggests that CDK5 is a unique member of this group. Unlike another important member of the family, CDK2, which plays a critical role in cell division cycle related diseases (e.g. cancer [3, 16, 17]), CDK5 has an indispensable role in the central nervous system. Deregulation of CDK5 activity by proteolytic conversion of p35 to p25 has been implicated in neurodegenerative diseases such as Alzheimer's disease, Parkinson's disease, etc [18–22]. In the past decades, many ATP-competitive inhibitors of cell cycle control related CDKs have been suggested [23–27], and several of them have progressed to clinical trials targeting diverse types of cancer. Within the CDK group of kinases, CDK inhibitors fall into three classes: those that are not selective for any specific CDK, those that inhibit CDK1, 2 and 5, and those that are selective for CDK4 and 6. Although specific inhibition of a protein kinase is highly desirable, it remains a challenge in drug design [26, 28–30]. No inhibitor that is selective for a single CDK has yet been discovered, probably due to the high degree of conservation of the amino acids lining the CDK ATP-binding pocket [31, 32].

The 20 important amino acids in the active sites of CDK1 and CDK2 are all the same, and 18 of these 20 amino acids are also found in CDK5, implying that most of

V. B. C. Tan (✉) · B. Zhang · K. M. Lim · T. E. Tay
Department of Mechanical Engineering,
National University of Singapore,
9 Engineering Drive 1,
117576 Singapore, Singapore
e-mail: mpetanbc@nus.edu.sg

the known inhibitors share similar binding patterns in these CDKs. New methods or mechanisms to explore new types of inhibitors with good selectivity are, therefore, considered highly desirable.

Normally, CDKs are activated in a two-step regulation [14, 33], namely, the binding of cyclins confers basal kinase activity, and phosphorylation of specific amino acids on the activation loop (T-loop) results in full activity. CDK5 is, however, fully activated only by binding of the activating proteins p35 or p39 with the T-loop via extensive interactions [15].

It has been reported that the activator protein p35 of CDK5 does not share detectable sequence similarity with the cyclins [15]. p35 binds CDK5 with exquisite selectivity but does not appreciably bind to or activate other members of the CDK family. A recent CDK5/p25 crystal structure [15] showed that p25, the truncated form of p35, presents a cyclin-box fold domain—the structural motif in the cyclins. The position of this domain relative to the kinase closely resembles that occupied by cyclin A when bound to CDK2. Recently, Pant et al. [34, 35] found that a further truncation of p25 (145–293) yields a CDK5 inhibitory peptide (CIP, 154–279) that can specifically inhibit CDK5/p25 activity by reducing the phosphorylation of tau in HEK293 cells. It has a higher binding affinity than p25 but does not affect the activity of CDK2. This suggests that CIP may act as a specific CDK5 inhibitor. The mechanism of inhibition remains unclear. In this work, the influences of the terminal truncations on p25 and CIP are investigated first by molecular dynamics (MD) simulations. Both MD simulations and molecular mechanics-Poisson-Boltzmann/surface area (MM-PBSA) energy decomposition are then established to help understand the properties of the CDK5/CIP/ATP/HHASPRK complex, because it has been reported that CDK5 shows a marked preference for a basic residue in the +3 position and phosphorylates the consensus sequence (S/T)PX(K/H/R), where S or T are the phosphorylatable serine or threonine, X is any amino acid and P is the proline residue in the +1 position. By comparing with our previous MD simulations of the CDK5/p25/ATP/HHASPRK complex and other reported results, the mechanism of inhibition of CIP is elucidated and suggestions for specific inhibition and the development of new selective peptide inhibitors with respect to CDKs are offered.

Methods

Molecular dynamics simulations

Molecular dynamics simulations were carried out using the SANDER module of AMBER 9.0 with the Cornell et al. all-atom force field [36]. Prior to the MD simulations, the values for some of the force field parameters for the ligands had to be developed because of the lack of reported data. Optimization of the ligands was first achieved with the Gassuian98 package at the HF/6-31G* theoretical level. Electrostatic potentials (ESP) were then generated with Merz-Singh-Kollman van der Waals parameters [37]. Fitting of the charges to the ESP was performed with the RESP program [38] of the AMBER package. GAFF [39] force fields parameters and RESP partial charges were assigned using the ANTECHAMBER module.

The starting geometry of p25 was generated from X-ray structures obtained from the Protein Data Bank (PDB ID code: 1UNL) [40]. CIP was obtained by truncating both ends of p25 in Accelrys Discovery Studio (Accelrys Discovery Studio v2.0.0.7264, Accelrys Software, http://accelrys.com/). CDK5/CIP/ATP/HHASPRK was derived from structure superimposition by sequence alignment with the Accelrys Discovery Studio software suite. To reflect actual experimental conditions, we docked the averaged structure of CIP together with CDK5/ATP/HHASPRK to investigate the influence of CIP on phosphate transfer reactions. ATP and HHASPRK were generated from the crystal structure of CDK2/cyclinA/ATP/HHASPRK. All simulations were performed at neutral pH. Lys and Arg residues were positively charged and Asp and Glu residues were negatively charged. The default His protonation state in Amber9 was adopted. Counter ions were added to maintain the electroneutrality of all the systems. Each system was immersed in a 10 Å layer truncated octahedron periodic water box. In all cases, the layer of water molecules contained around 11,000 TIP3P [41] water molecules in each of the complexes. A 2 fs time step was used in all the simulations and long-range electrostatic interactions were treated with the particle mesh Ewald (PME) procedure [42] using a cubic B-spline interpolation with a 10^{-5} tolerance for the direct-space and a 12 Å non-bonded cutoff. Bond lengths involving hydrogen atoms were constrained using the SHAKE algorithm [43]. All systems were minimized prior to the production run. To further verify the calculations, MD simulations of CIP and CDK5/CIP/ATP/HHASPRK were carried out with two different minimization and heating strategies (set 1 and 2) to generate different starting configurations of the protein systems for the production computations to investigate the influence of the truncations. The minimization steps of simulation set 1 of CIP and CDK5/CIP/ATP/HHASPRK, performed with the SANDER module under constant volume conditions, consisted of four steps. All heavy atoms in both proteins and ligands were restrained with degressive forces of 500, 100, and 5 kcal mol^{-1} $Å^{-1}$, respectively. In the first three steps, minimization of the solvent molecules and hydrogen atoms of the systems involved 250 cycles of steepest descent followed by 250

cycles of conjugate gradient minimization. All systems were then relaxed by 500 cycles of steepest descent and 1,000 cycles of conjugate gradient minimization in the last step. Then, after a 2 ps MD relaxation under NPT conditions, the whole system was heated to 300 K in steps. The system was first heated to 100 K during 10 ps and then to 200 K during the next 10 ps, and then to 250 K in another 10 ps. Finally, it was heated to 300 K in the last 20 ps. p25 was preprocessed with the set 1 minimization and heating strategy.

In simulation set 2, all the heavy atoms of CIP and CDK5/CIP/ATP/HHASPRK were restrained with forces of 100 and 5 kcal mol^{-1}, respectively. The systems were minimized with 250 cycles of steepest descent followed by 250 cycles of conjugate gradient minimization. All systems were then relaxed by 1,000 cycles of steepest decent and 1,500 cycles of conjugate gradient algorithms. Finally, they were heated directly to 300 K in 30 ps.

The production parts of all the systems took 10 ns (except for CDK5/CIP/ATP/HHASPRK in simulation set 2, which spanned 12.5 ns) in the NPT ensemble at 300 K with Berendsen [44] temperature coupling and constant pressure (1 atm) with isotropic molecule-based scaling [44].

MM-PBSA calculations

Binding free energies and energy decomposition of all systems were analyzed using the MM-PBSA [45] approach to highlight the electrostatic and van der Waals contributions to the binding of ATP, substrate and ion with the kinase.

The binding free energies (ΔG_{bind}) were computed as:

$$\Delta G_{bind} = \Delta G(complex) - [\Delta G(protein) + \Delta G(ligand)] \quad (1)$$

$$\Delta G_{bind} = \Delta E_{gas} + \Delta\Delta G_{solv} - T\Delta S \quad (2)$$

$$\Delta E_{gas} = \Delta E_{int} + \Delta E_{ele} + \Delta E_{vdw} \quad (3)$$

$$\Delta G_{solv} = \Delta G_{pb} + \Delta G_{nonpolar} \quad (4)$$

The sum of molecular mechanical energies, ΔE_{gas}, can be divided into contributions from internal energy (ΔE_{int}), electrostatic potential (ΔE_{ele}) and van der Waals (ΔE_{vdw}) potential. The solvation free energy (ΔG_{solv}) is composed of two parts: polar solvation free energy (ΔG_{PB}) and nonpolar salvation free energy ($\Delta G_{nonpolar}$). All energies are averaged along the MD trajectories. The snapshots of each system were sampled from the last 8 ns single trajectory with an interval of 50 ps. The single trajectory approach was applied to estimate the energies. Estimation of energies in this manner has proven successful in our previous [46–48] and many other studies [49–51]. Part of the reason for the success of this approach is the cancellation of errors, which masks the effect of incomplete sampling. A logically better approach is the use of separate trajectories of protein–ligand complex, free protein and free ligand. Unfortunately, due to sampling limitations, the separate trajectories approach appeared to be significantly less stable in numerical studies [49]. E_{gas} was obtained using SANDER, and estimation of ΔG_{PB} was conducted with a built-in module, PBSA, in AMBER. $G_{nopolar}$ was determined from Eq. 5,

$$\Delta G_{nopolar} = \gamma A + b \quad (5)$$

where A is the solvent-accessible surface area estimated using Sanner's algorithm [52] with a solvent probe radius of 1.4 Å and the PARSE atomic radii parameters [53]. In Eq. 5, γ and b are empirical constants and are set to 0.00542 kcal mol^{-1} $Å^{-2}$ and 0.92 kcal mol^{-1}, respectively.

Results and discussion

Influence of truncation of p25 on the conformation of CIP

CIP (154–279) is a N- and C-terminal-truncated form of p25 (145–293). According to the crystal structure of the CDK5/p25 complex and our previous MD simulations [47, 54], intensive and stable hydrophobic interactions exist between the N terminal (Thr148, Leu299, Leu300), C terminal (Phe282, Val285, Phe286, Leu289) and α2 (Pro198, Ala199, Val202, Tyr205) helices of p25 (helices named according to Tarricone et al. [15]). These stabilize the conformation of the protein during the long-term dynamic process. Truncation of p25 to CIP might lead to severe impairment of these interactions. Therefore, CIP, p25 and CDK5/CIP/ATP/HHASPRK were entered into long-time MD simulations to investigate the influence of these truncations on the conformation. To show that the simulation results are not overly sensitive to the initial configurations, different preprocessing strategies were employed to give different initial configurations of CIP and CDK5/CIP/ATP/HHASPRK for the production run. Initially, the conformation of the proteins was analyzed to explore the effect of the truncations. Similar behavior of a motif in CIP were detected in both the simulation sets.

Figure 1 (a,b) shows that both sets of simulations with the two different strategies reflect some degree of fluctuation of the CIP conformation. Comparing the averaged structures from MD simulations of CIP and that of p25

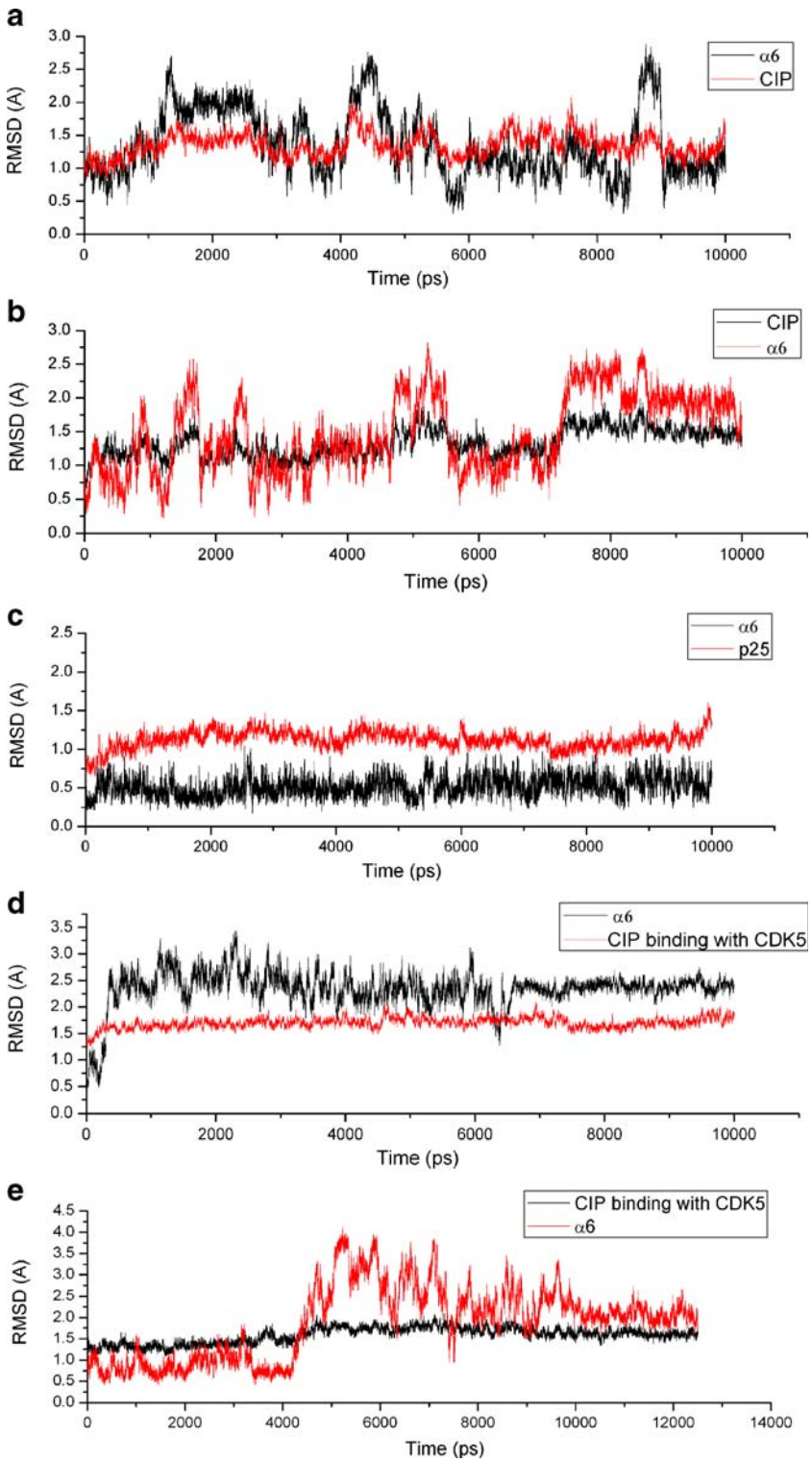

Fig. 1 Root mean squares deviation (RMSD) of **a** α6 and CIP (simulation set 1, as described in Methods), **b** α6 and CIP (simulation set 2), **c** α6 and p25, **d** α6 and CIP when complex with CDK5/ATP/HHASPRK (simulation set 1), and **e** α6 and CIP when complex with CDK5/ATP/HHASPRK (simulation set 2)

reveals an obvious displacement of α6. The relatively oscillatory RMSD curves of the helix in CIP (Fig. 1) and the flat curve of α6 in p25 (Fig. 1c) seem to indicate that fluctuation of the helix is one of the causes of the CIP motion. The curves in Fig. 1a,b show that it is very hard for α6 to remain in its original position as in p25, and that part of the helix unfolds into a small coil in the absence of stabilizing forces from the interactions between the C/N termini and C-terminal/α2 helix. However, when combined with CDK5 in CDK5/CIP/ATP/HHASPRK, α6 presents a stable conformation in the complex after an initial obvious displacement and fluctuation. As seen in Fig. 1d and e, the

Table 1 Energy contribution of the T-loop and the α-helix of cyclin-dependent kinase (CDK) 5 to the binding of CDK5/p25/ATP/HHASPRK and CDK5/CIP/ATP/HHASPRK. Values are in kcal mol^{-1}. *VDW* van der Waals, *ELE* electrostatic, *TOT* total

	T-loop			α-helix		
Interactions	VDW	ELE	TOT	VDW	ELE	TOT
CDK5/p25/ATP/HHASPRK	−66.44	−371.63	−212.3	−58.16	−285.84	−412.94
CDK5/CIP/ATP/HHASPRK	−63.36	−332.17	−203.54	−70.71	−414.02	−426.06

results of the different simulation sets reveal similar changes in the helix; after an apparent movement in each production run, the helix slowly adopts a stable position and conformation after about 6 ns (0.3–6.3 ns in simulation set 1, Fig. 1d, 4.2–10 ns in set 2, Fig. 1e). The relatively long duration of fluctuations of α6 might be due to the very flexible coil at the end of the helix. Hence, from both MDs it seems that some interactions from CDK5 with CIP could maintain the helix in a steady environment. Considering the very similar displacement and conformational changes seen in MDs with different initial configurations of CIP and CDK5/CIP/ATP/HHASPRK, the following discussion, which is based on results from simulation set 1, can also be applied to other configurations.

In the CDK5/CIP/ATP/HHASPRK combination, it was found that amino acids Glu274, Asn276 and Asp278 shift toward the α3 direction by 6.82 Å, 6.55 Å and 8.46 Å, respectively, due to displacement of α6. This means that the α6 and α helix (45–51) of CDK5 are much closer together than they are in the CDK5/p25/ATP/HHASPRK complex, and that more electrostatic interactions occur between α6 and the helix (45–51). The energy decomposition calculations also show that the interactions contributed from the α helix (45–51) are larger than those in the CDK5/p25/ATP/HHASPRK complex (Table 1).

Influence of truncation on the hydrophobic pocket accommodating Ile153

The hydrophobic binding pocket lined by residues Ala199, Met237, Ile275, Ala277, Pro279 and Phe282 of p25 has been reported [15] to be very important for accommodating Ile153 on the CDK5 activation loop (the T-loop) that is crucial for the activation of CDKs. The recognition and binding of Ile153 may contribute to the stabilization of the T-loop and the selectivity of CDK5/p25. In CIP, however, Pro279 and Phe282 are truncated from the N terminus, so their interactions with Ile153 are missing. Ile275 and Ala277 are displaced away from their original locations due to the displacement of α6 and, consequently, the helix displaces slightly from its original position due to the lack of strong interactions between the N/C terminals and the α2 helix. The displacement causes a 5.14 Å shift of Ala199 compared to its position in p25. All these changes in the positions of the residues result in changes in both the shape and location of the hydrophobic pocket, as seen in Fig. 2.

The displacement and unfolding of the α6 helix also cause the T-loop to be pushed away from its original position in the CDK5/p25/ATP/HHASPRK complex (Fig. 2). Moreover, the conformation of the loop is also distorted during the simulations. For instance, the displacements of Ile153 and Arg156 are 5.57 Å and 5.65 Å, respectively. Due to the variations in the hydrophobic pocket in p25, Ile153 cannot reside at its original location. Instead, it remains outside the new pocket with a different side chain conformation as shown in Fig. 2. All the changes seem to impact the interaction between the T-loop and CIP. For example, the van der Waals contribution from the side chain of Ile153 in CDK5/p25/ATP/HHASPRK and CDK5/CIP/ATP/HHASPRK is −3.64 and −1.71 kcal mol^{-1}, respectively, and the electrostatic contributions from the side chain of Ser159 in CDK5/p25/ATP/HHASPRK and CDK5/CIP/ATP/HHASPRK are −11.17 and −1.77 kcal mol^{-1}, respectively. Hence, with the distortion and displacement of the T-loop, the contributions of the two important interacting residues are apparently impaired. Energy decomposition calculations of the contribution of the T-loop to the CDK5/p25 and CDK5/CIP bonds are consistent with the results of Ile153 and Ser159, as seen in Table 1. A comparison of the

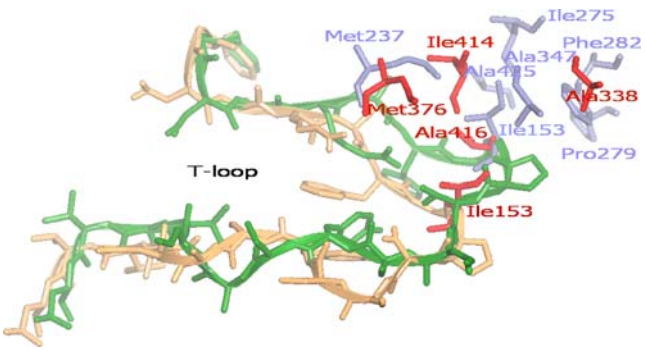

Fig. 2 Displacement of the T-loop and the hydrophobic pocket for Ile153. The T-loop of CDK5 and the hydrophobic pocket for Ile153 of p25 and CIP in CDK5/p25/ATP/HHASPRK and CDK5/CIP/ATP/HHASPRK are colored *orange/yellow* and *green/blue*, respectively. Ile153s on the T-loops of CDK5/p25/ATP/HHASPRK and CDK5/CIP/ATP/HHASPRK are highlighted with *orange* and *green*, respectively

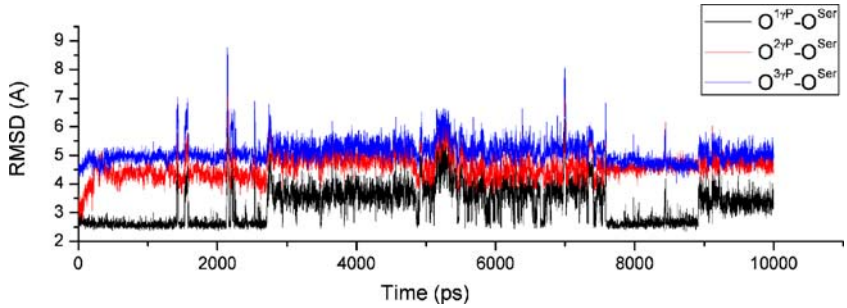

Fig. 3 Distances between $O^{1\gamma P}$ and O^{Ser}

van der Waals and electrostatic contributions of the T-loop in both complexes shows that the T-loop does not bind as tightly in CDK5/p25 as when binding with CIP. It seems that truncation of the termini affects the shape and position of the hydrophobic pocket binding with Ile153. As a result, Ile153 cannot recognize and fit snugly into CIP. It has been reported that Ile153 is critical for association with p25 and could contribute to the selectivity of the CDK5/p35 interaction, and that the T-loop is crucial for the activation of CDK5. Changes to the hydrophobic pocket might, therefore, affect activation of the kinase.

According to our MD simulations, it seems there is no other obvious conformational deviation apart from the influence of the CIP on the T-loop. From the structure of CDK5/p25, it can be seen that two important motifs in CDK5, namely the α-helix (45–51) and the T-loop (145–165), contribute to the most important interactions with p25. The energy decomposition calculations are listed in Table 1. As mentioned previously and as shown in the table, both the van der Waals and electrostatic contributions from α-helix (45–51) are increased significantly due to the displacement of α6, resulting in tighter interactions between the two helices. According to experimental results, CIP exhibits higher affinity for CDK5 than p25. The decreased binding affinity between the T-loop of CDK5 and CIP according to energy calculations seems to be compensated by tighter binding with other parts of the kinase.

CIP inhibition of the phosphate transfer reaction

From both the crystal structure of pT160CDK2/cyclinA/ATP/HHASPRK [55] and our previous MD simulations on CDK5/p25/ATP/HHASPRK [47], a suitably shaped pocket with an unfavorable Val164 conformation of CDK2 or CDK5 is specific for a proline at the P+1 position. In the present system, the shape of the valine pocket is intact because of the displacement and distortion of the T-loop. However, the pocket is displaced slightly from its original position, which might affect how the proline is accommodated. Consequently, the substrate peptide HHASPRK cannot be properly held in the binding site. The displacements of the α carbon atoms of the substrate residues (HHASPRK) are 3.22, 2.08, 4.78, 6.47, 9.78, 10.91 and 13.58 Å, respectively. This means that the movement of the N-terminus of the substrate is smaller than that of the C-terminus. The strong hydrogen bonding phosphate groups of ATP($O^{\gamma P}$) continue to exist throughout the whole dynamic process (Fig. 3). This might drag the peptide

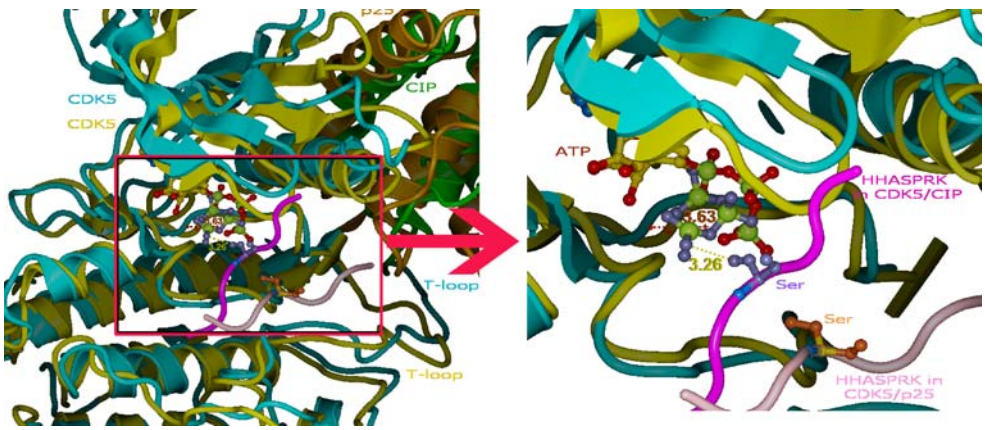

Fig. 4 *Left* Original positions of ATP and HHASPRK peptide in CDK5/p25/ATP/HHASPRK, *right* original and displaced substrate HHASPRK (*purple/yellow*), ATP (*multicolored/dark gray*) and magnesium ion (*red star shape*) in CDK5/p25/ATP/HHASPRK and CDK5/CIP/ATP/HHASPRK. The serine on the original and displaced HHASPRK are also depicted on the right. Distances between O^{Ser} of the serine and the γP of ATP in CDK5/p25/ATP/HHASPRK and CDK5/CIP/ATP/HHASPRK and the displacement of the ion are 4.06, 3.25 and 3.63 Å, respectively

away from the binding site and, in addition, distort the conformation of the phosphate group of ATP. At the same time, a closer look at the topology of the substrate and the CDK5/CIP structure shows that the C-terminus is the end closest to CIP (Fig. 4), which probably indicates that fluctuation of the truncated activator during MD simulations affects the interactions between the substrate and CIP itself. From Fig. 4, it is clear that both the long phosphate side chain and the magnesium ion adopt new positions after 10 ns of MD simulations. The displacement of the γP and the ion are 3.96 and 3.63 Å, respectively, whereas the CDK5 part maintains a perfectly steady conformation. It has been proven that the correct coordination around the magnesium from amino acids Asn131 and Asn144 is crucial for the phosphate transfer reaction [47, 54]. In CDK5/p25/ATP/HHASPRK, the coordination between OD1 of Asn131 and Asn144 is 2.11 and 1.93 Å, respectively. However, after displacement of the ion, the distances to the ion and the oxygen atoms are 5.29 and 7.00 Å, respectively, which means the ion has a different and improper coordination environment due to displacement of the phosphate group and the ion itself; consequently, the phosphate transfer does not seem to happen.

Conclusions

In this work, the influence of N and C terminal truncations of p25 on the binding of CDK5 and the substrate peptide HHASPRK was explored through MD simulations and energy decomposition calculations. Interactions among the N and C termini and the α2 helix of p25 were first investigated. It turns out that, without the interactions, the α6 helix of p25 fluctuates continuously during the dynamic process, and, because of the truncation and fluctuations, the hydrophobic pocket accommodating Ile153 from the T-loop of p25 is also distorted and can no longer bind the hydrophobic amino acid. Binding energy contributions from the T-loop to the CDK5/CIP complex are, thus, lowered. However, energy decomposition calculations indicate that reduction of the binding energy in the T-loop area can be compensated by other enhanced interactions, for example, the α helix (45–51) of CDK5.

Due to the displacement of the α6 helix, the conformation of the T-loop of CDK5 is distorted and pushed away from its original position. As a result, the substrate peptide HHASPRK cannot be held in the binding site. During the displacement of the substrate, the strong hydrogen bond formed between O^{Ser} and $O^{\gamma P}$ also drags the phosphate chain of ATP and the magnesium ion away from their original locations. Without a proper coordination environment around the ion, the phosphate transfer reaction does not seem to occur.

Our work leads us to suggest new ways to inhibit CDK5 by disrupting the interactions between the crucial hydrophobic interactions between Ile153 on the T-loop of CDK5 and the activator to prevent complete activation of the kinase. Groups or substituents impairing or replacing those important hydrophobic interactions might selectively inhibit CDK5 but without any influence on activity of other CDKs.

References

1. De Azevedo WF, Mueller-Dieckmann HJ, Schulze-Gahmen U, Worland PJ, Sausville E, Kim SH (1996) Proc Natl Acad Sci USA 93:2735–2740
2. De Azevedo WF, Leclerc S, Meijer L, Havlicek L, Strnad M, Kim SH (1997) Eur J Biochem 243:518–526
3. Harper JW, Adams PD (2001) Chem Rev 101:2511–2526
4. Hunter T, Pines J (1994) Cell 79:573–582
5. Norbury C, Nurse P (1992) Annu Rev Biochem 61:441–470
6. Sherr C (1996) Science 274:1672–1677
7. Baumann K, Mandelkow EM, Biernat J, Piwnica-Worms H, Mandelkow E (1993) FEBS Lett 336:417–424
8. Hisanaga S, Ishiguro K, Uchida T, Okumura E, Okano T, Kishimoto T (1993) J Biol Chem 268:15056–15060
9. Lew J, Winkfein RJ, Paudel HK, Wang JH (1992) J Biol Chem 267:25922–25926
10. Johnson LN, Lewis RJ (2001) Chem Rev 101:2209–2242
11. Niethammer M, Smith DS, Ayala R, Peng J, Ko J, Lee MS, Morabito M, Tsai LH (2000) Neuron 28:697–711
12. Paudel HK, Lew J, Ali Z, Wang JH (1993) J Biol Chem 268:23512–23518
13. Shuang RQ, Zhang L, Fletcher A, Groblewski GE, Pevsner J, Stuenkel EL (1998) J Biol Chem 273:4957–4966
14. Jeffrey PD, Russo AA, Polyak K, Gibbs E, Hurwitz J, Massagué J, Pavletich NP (1995) Nature 376:313–320
15. Tarricone C, Dhavan R, Peng J, Areces LB, Tsai LH, Musacchio A (2001) Mol Cell 8:657–669
16. Garrett MD, Fattaey A (1999) Curr Opin Genet Dev 9:104–111
17. Webster KR (1998) Expert Opin Invest Drugs 7:865–887
18. Bu B, Li J, Davies P, Vincent I (2002) J Neurosci 22:6515–6525
19. Lau LF, Ahlijanian MK (2003) 12:209–214
20. Nguyen MD, Julien JP (2003) Neurosignals 12:215–220
21. Smith PD, Crocker SJ, Jackson-Lewis V, Jordan-Sciutto KL, Hayley S (2003) Proc Natl Acad Sci USA 100:13650–13655
22. Wang J, Liu S, Fu Y, Wang JH, Lu Y (2003) Nat Neurosci 6:1039–1047
23. Crews CM, Mohan R (2000) Curr Opin Chem Biol 4:47–53
24. Huew A, Mazitschek R, Giannis A (2003) Angew Chem Int Ed 42:2122–2138
25. Knockaert M, Greengard P, Meijer L (2002) Trends Pharmacol Sci 23:417–425
26. Sausville EA (2002) Trends Mol Med 8:S32–S37
27. Sielecki TM, Boylan JF, Benfield PA, Trainor GL (2000) J Med Chem 43:1–18
28. Leclerc S, Garnier M, Hoessel R, Marko D, Bibb JA, Snyder GL, Greengard P, Biernat J, Wu YZ, Mandelkow EM, Eisenbrand G, Meijer L (2001) J Bio Chem 276:251–260
29. Noble MEM, Endicott JA, Johnson LN (2004) Science 303:1800–1805
30. Noble M, Barrett P, Endicott J, Johnson L, McDonnell J, Robertson G, Zawaira A (2005) Biochim Biophys Acta 1754:58–64

31. Honma T, Hayashi K, Aoyama T, Hashimoto N, Machida T, Fukasawa K, Iwama T, Ikeura C, Ikuta M, Suzuki-Takahashi I, Iwasawa Y, Hayama T, Nishimura S, Morishima H (2000) J Med Chem 44:4615–4627
32. Honma T, Yoshizumi T, Hashimoto N, Hayashi K, Kawanishi N, Fukasawa K, Takaki T, Ikeura C, Ikuta M, Suzuki-Takahashi I, Hayama T, Nishimura S, Morishima H (2001) J Med Chem 44:4628–4640
33. Russo A, Jeffrey PD, Pavletich NP (1996) Nat Struct Biol 3:696–700
34. Amin ND, Albers W, Pant HC (2002) J Neurosci Res 67:354–362
35. Zheng YL, Li BS, Amin ND, Albers W, Pant HC (2002) Eur J Biochem 269:4427–4434
36. Cornell WD, Cieplak P, Bayly CI, Gould IR, Merz KM, Ferguson DM Jr, Spellmeyer DC, Fox T, Caldwell JW, Kollman PA (1995) J Am Chem Soc 117:5179–5197
37. Besler BH, Merz KM, Kollman PA (1990) J Comput Chem 11:431–439
38. Fox T, Kollman PA (1998) J Phys Chem B 102:8070–8079
39. Case DA, Pearlman DA, Caldwell JW, Cheatham TE III, Wang J, Ross WS, Simmerling CL, Darden TA, Merz KM, Stanton RV, Cheng AL, Vincent JJ, Crowley M, Tsui V, Gohlke H, Radme RJ, Duan Y, Pitera J, Massova I, Seibel GL, Singh UC, Weiner PK, Kollman PA (2002) AMBER 7. University of California, San Francisco
40. Mapelli M, Massimiliano L, Crovace C, Seeliger MA, Tsai LH, Meijer L, Musacchio A (2005) J Med Chem 48:671–679
41. Jorgensen WL, Chandrasekhar J, Madura JD, Impey RW, Klein ML (1983) J Chem Phys 79:926–935
42. Darden T, York D, Pedersen L (1993) J Chem Phys 98:10089–10092
43. Ryckaert JP, Ciccotti G, Berendsen HJC (1977) J Comput Phys 23:327–341
44. Berendsen HJC, Postma JPM, van Gunsteren WF, Dinola A, Haak JR (1984) J Chem Phys 81:3684–3690
45. Massova I, Kollman PA (2000) Perspect Drug Discov 18:113–135
46. Zhang B, Tan VBC, Lim KM, Tay TE (2006) J Comput Aided Mol Des 20:395–404
47. Zhang B, Tan VBC, Lim KM, Tay TE (2007) Biochem 46:10841–10851
48. Zhang B, Tan VBC, Lim KM, Tay TE, Zhuang SL (2007) J Mol Model 13:79–89
49. Bao J, Zhang DW, Zhang JZ, Huang PL, Huang PL, Lee-Huang S (2007) FEBS Lett 581:2737–2742
50. Hou TJ, Guo SL, Xu XJ (2002) J Phys Chem B 106:5527–5535
51. Zhuang SL, Zou JW, Jiang YJ, Mao X, Zhang B, Liu HC, Yu QS (2005) J Med Chem 48:7208–7214
52. Sanner MF, Olson AJ, Spehner JC (1996) Biopolymers 38:305–320
53. Sitkoff D, Sharp KA, Honig B (1994) J Phys Chem 98:1978–1988
54. Zhang B, Tan VBC, Lim KM, Tay TE (2007) J Chem Info Model 47:1877–1885
55. Cook A, Lowe ED, Chrysina ED, Skamnaki VT, Oikonomakos NG, Johnson LN (2002) Biochemistry 41:7301–7311